PERFORMANCE OF A TEN-STAGE ELECTROSTATIC DEPRESSED COLLECTOR FOR KLYSTRONS

W. Neugebauer, Microwave Tube Operation
and
T. G. Mihran, Research and Development Center
General Electric Company
Schenectady, New York

The improvement of the efficiency of microwave tubes is important from at least two points of view. First, for a given rf power output, a more efficient tube means, of course, that a smailer prime power source can be used; a second important advantage is that a more efficient tube allows use of a smaller heat rejection system. Both of these features take on additional significance when the tube is to be used in a space application. High efficiency is also important in some ground-based applications, such as linear accelerators designed for cw operation.

There are two approaches to achieving high efficiency in a microwave tube. First, you can improve and optimize the electronic efficiency of the basic microwave interaction, whether it be a klystron, a TWT, or a crossed-field device. For example, two papers were given at this conference last year showing that the efficiency of klystrons intended for narrowband, FM applications could be increased to the 60 to 70% range. There are other applications, however, in which use of these optimum klystron designs is not feasible. Two examples are: (1) klystrons intended for AM service, and (2) broadband klystrons. In both cases it is necessary to compromise the optimum design conditions, and efficiency falls below 40%, and sometimes to as low as 20%.

It is in these inherently low efficiency applications that the development of another means of increasing tube efficiency becomes essential. If the application dictates low interaction efficiency, one can turn to the idea of recovering some of power normally wasted as heat in the collector region of the tube.

The work we will describe today shows that it is possible to increase the net power conversion efficiency of a klystron from a base value of 45% to over 65% by use of a carefully designed electrostatic depressed collector. Furthermore, this improvement in net tube efficiency can be achieved over a two-to-one range of base tube efficiencies, indicating that the depressed collector is directly applicable to AM klystron service. A depressed collector is also useful on a high efficiency klystron. A well designed collector can raise the efficiency of a narrow band FM tube from 70 to over 80 percent.

The first slide summarizes past work on depressed collectors. In this slide the net tube efficiency with collector depression, η, is plotted against the base tube efficiency without depression, η_o. The solid points were measured on klystrons; the hollow points are TWT measurements. It is evident that if one is dealing with fairly efficient tubes, say with η_o greater than 40%, it has not been possible in the past to increase tube efficiency by more than 10 percentage points. For less efficient tubes, the addition of 15 to 20 percentage points seems to be the rule, although there are in this region two reports of exceptional performance.

For the most part these results were obtained using one or two stages of collector depression. Since we were interested in recapturing the energy from the spent beam of a klystron, which inherently has a wider spectrum of energies than a TWT, we felt it was essential to increase the number of electrodes to at least five, and possibly to as many as ten. To place this

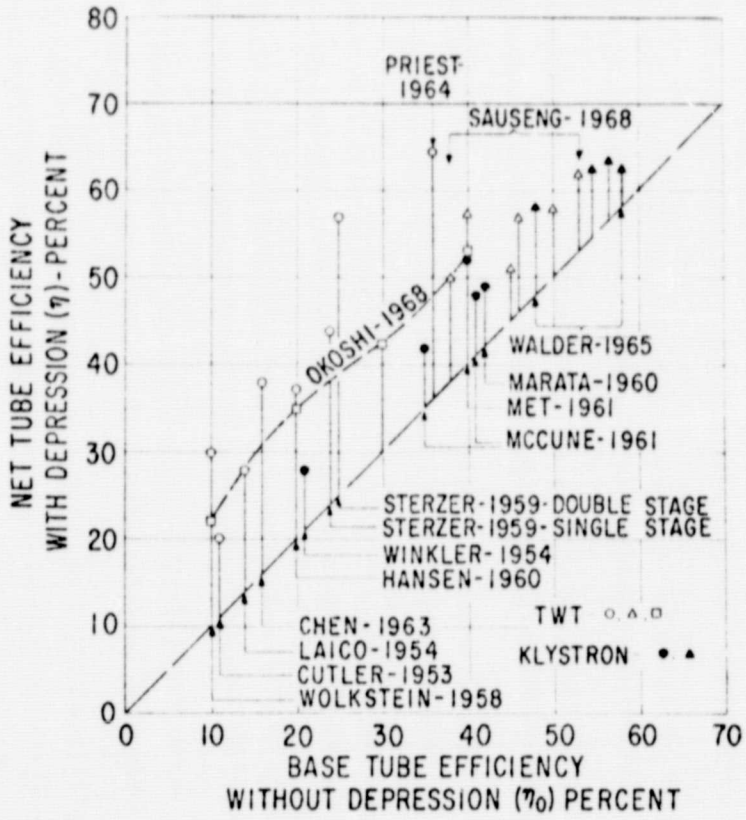

Efficiency with Depression versus Undepressed Efficiency

number of electrodes in their optimum positions, it was essential to calculate a large catalog of electron trajectories for electrons of different input energies and with a variety of initial conditions.

The first of two collectors constructed for this project established the validity of the computer design methods. A final collector built subsequently incorporated several design changes based on this computer analysis.

Before describing the collector performance, some basic parameters will be defined. A schematic diagram for the depressed collector test set is shown in the next slide. The tube was a commercial half-perv, one kilowatt CW, 750 MHz, three cavity klystron with an insulated collector. The original collector was removed and this slide shows the approximate shape of the interim collector, with its four cone-shaped collecting electrodes, a back cup, and a dispersing spike. The beam voltage, variable from 1 to 9 kv was obtained from a oversized supply, and the collector electrode voltages were obtained from a tapped bleeder resistor bank.

The recovered collector power was measured by multiplying the electrode currents I_1 through I_4 and I_{SC} by their respective electrode voltages. Rf power output was measured calorimetrically, and all dc meters were calibrated.

The net tube efficiency is obtained by measuring the rf power output in the water load (next slide), correcting it for the circuit efficiency (approximately 90%), and dividing it by the net dc power input to the tube. This is obtained by subtracting the sum of the powers recovered at the various electrodes from the undepressed dc power input $I_c V_c$.

Base tube efficiency is obtained by neglecting the recovered power sum. This is how the tube would operate without a depressed collector.

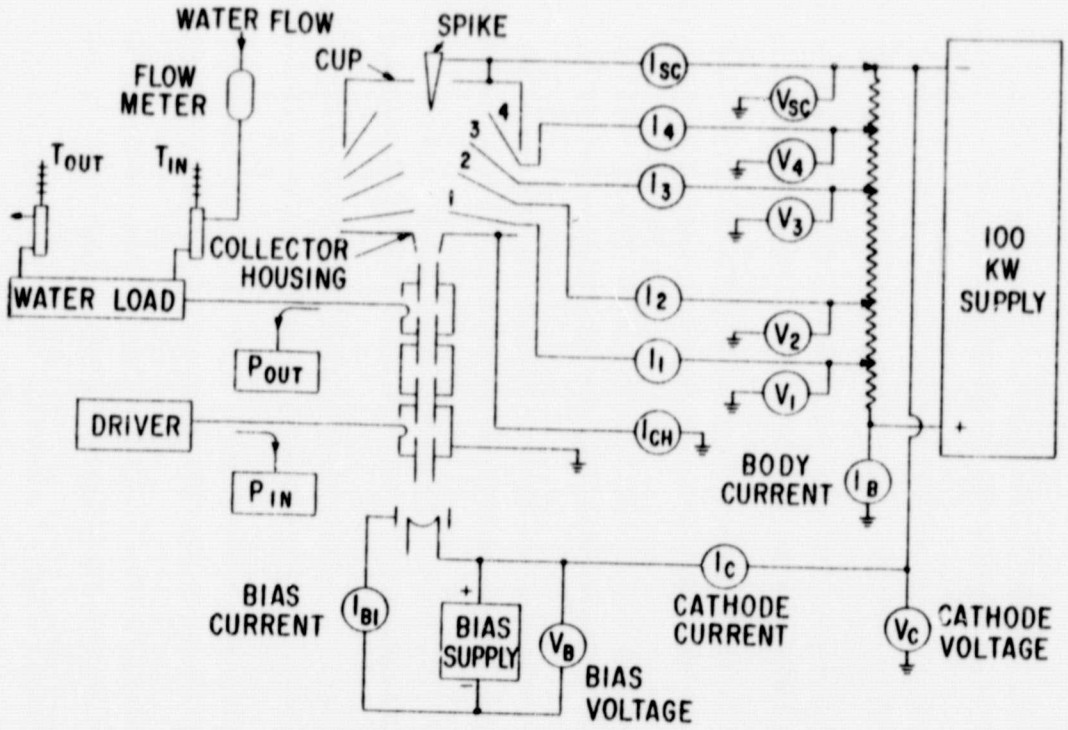

Test Set Circuit

NET TUBE EFF. $$\eta = \frac{P_{ext}/\eta_{ckt}}{I_c V_c - \sum_{i=1}^{5} I_i V_i}$$

BASE TUBE EFF. $$\eta_o = \frac{P_{ext}/\eta_{ckt}}{I_c V_c}$$

COLLECTOR EFF. $$\eta_c = \frac{\sum_{i=1}^{5} I_i V_i}{(1-\eta_o) I_c V_c - V_c I_{int-dc} - 0.5 V_c I_{int-rf}}$$

Definitions of Efficiency

Finally, rf collector efficiency is obtained by dividing the recovered power sum by the spent beam power input to the collector. To be completely accurate one should not charge the collector with beam power intercepted under dc conditions, so this quantity is subtracted from the denominator. Another correction involves the subtraction of a term due to additional current interception under rf conditions. However, this correction involved estimation of the intercepted energy and the final results will be presented both with and without it.

A set of electron trajectories calculated with our analog computer for the interim collector is shown on the next slide. The dispersing spike and the back cup are run at cathode potential, thus diverting the beam into the radial direction, and eventually reflecting it. Electron trajectories were first established using just the empty box as the retarding system. Then the equipotentials were plotted, and ~~five~~ 4 electrodes were placed on top of their corresponding equipotentials. The locus of the electrode edges was chosen so that most of the electrons hit on the top side of their collecting electrode. In this way secondary emission is suppressed because the electrons are accelerating as they strike the surface. It was on the basis of a limited investigation of this type that the interim collector was designed and built.

After extensive tests of the interim collector, we returned to the computer and ran a more complete set of over three hundred electron trajectories. From these, a "bean count" could be made to establish the anticipated current to each electrode as a function of beam energy. The computed electrode currents are shown in the next slide.

Idealized current behavior is shown in this slide by the dashed rectangular boxes, the current switching from one electrode to the next electrode

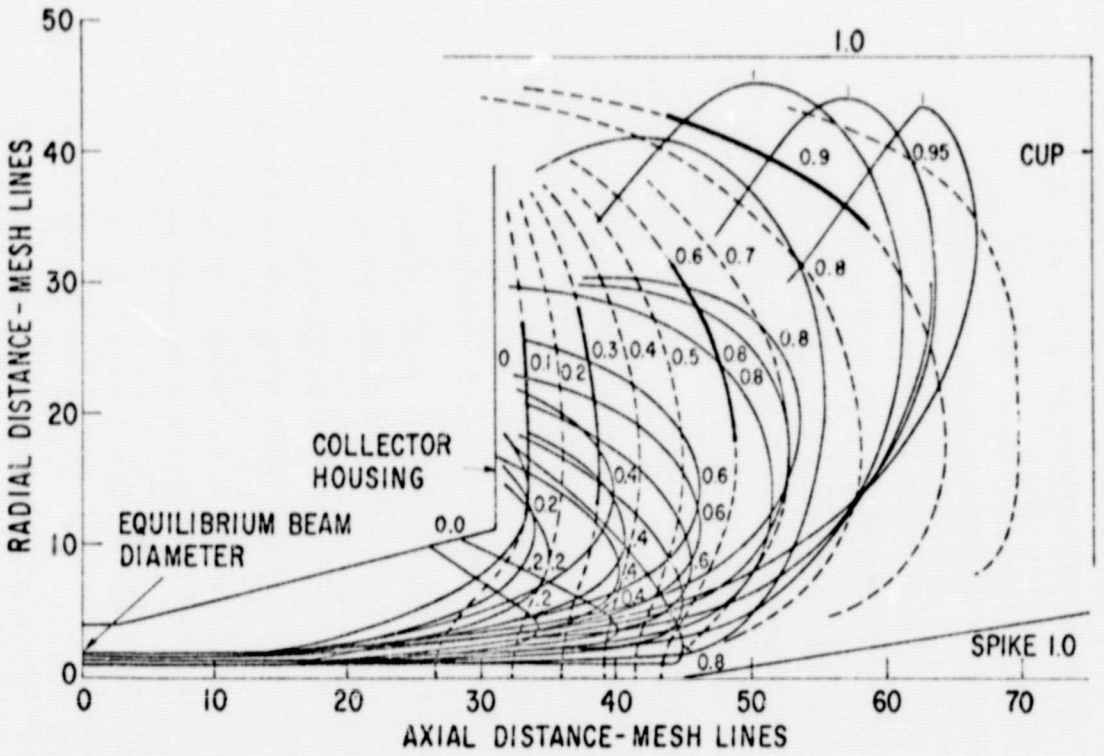

Interim Collector Trajectories

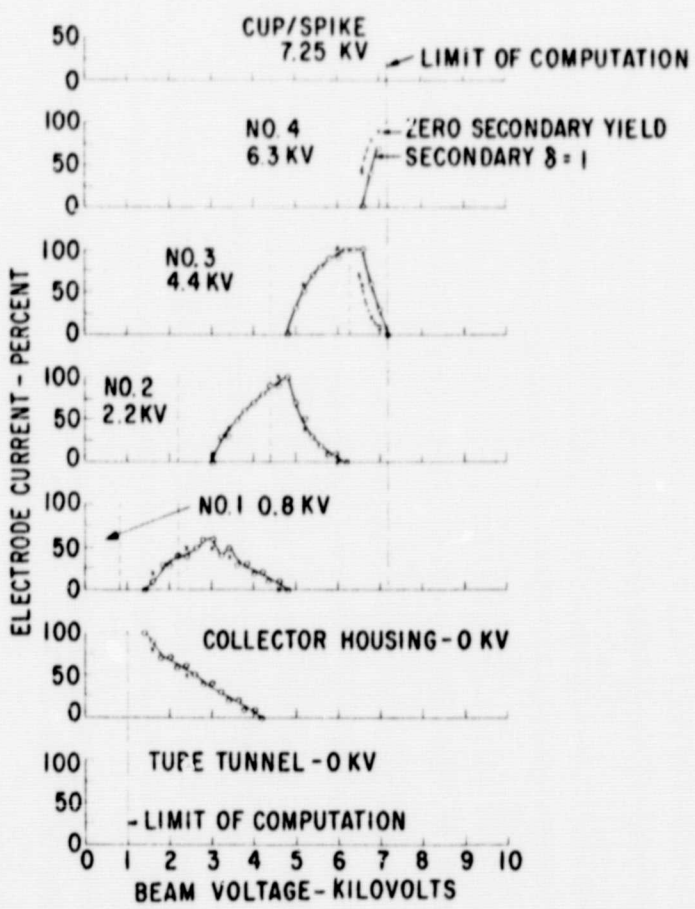

Computed Current Division of Interim Collector

as the beam voltage exceeds first one electrode potential and then another. From the computed points we see that triangular rather than rectangular current distributions are predicted and that these are offset appreciably to the right in all cases.

Let's now compare these computed results with the current distributions that we measured (next slide). The general agreement is excellent between computed and measured results. The minor discrepancies that are present can be explained for the most part by secondary electron effects. The most important of these discrepancies are these two measured bumps in the current to electrodes #3 and #4 at high beam voltage. Ideally, this current should have been recovered at 7.25 kv and not at these lower voltages. This was an important clue to improvement of the final collector.

Let us move now to a more practical but less revealing level of agreement between theory and experiment. By choosing a fixed dc beam voltage and summing the powers recovered at each electrode, we can calculate the dc collector efficiency as a function of beam voltage using these current division curves. This leads to the measured and computed curves shown on the next slide. Note that the measured collector efficiency approaches 80% at the design voltage of 7 kv. However, as the beam voltage is reduced below or raised above this design value, collector efficiency drops significantly.

The dashed computed curve shown in this slide is in good agreement with the measured curve. The major discrepancy is the presence of these "icicles" on the measured curve. The computed curve has been calculated assuming that the secondary yield is unity. These icicles in the measured curve are caused by secondary yields in excess of unity due to grazing incidence at certain beam voltages.

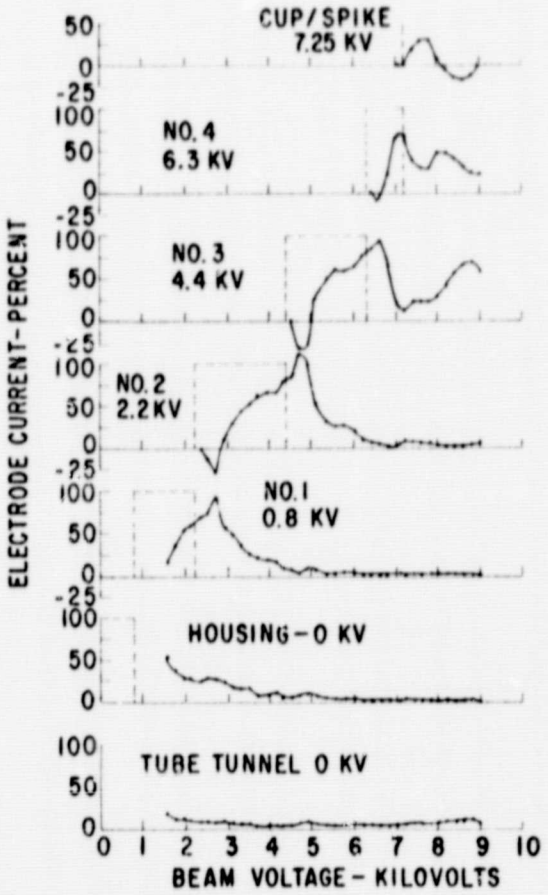

Measured Current Division of Interim Collector

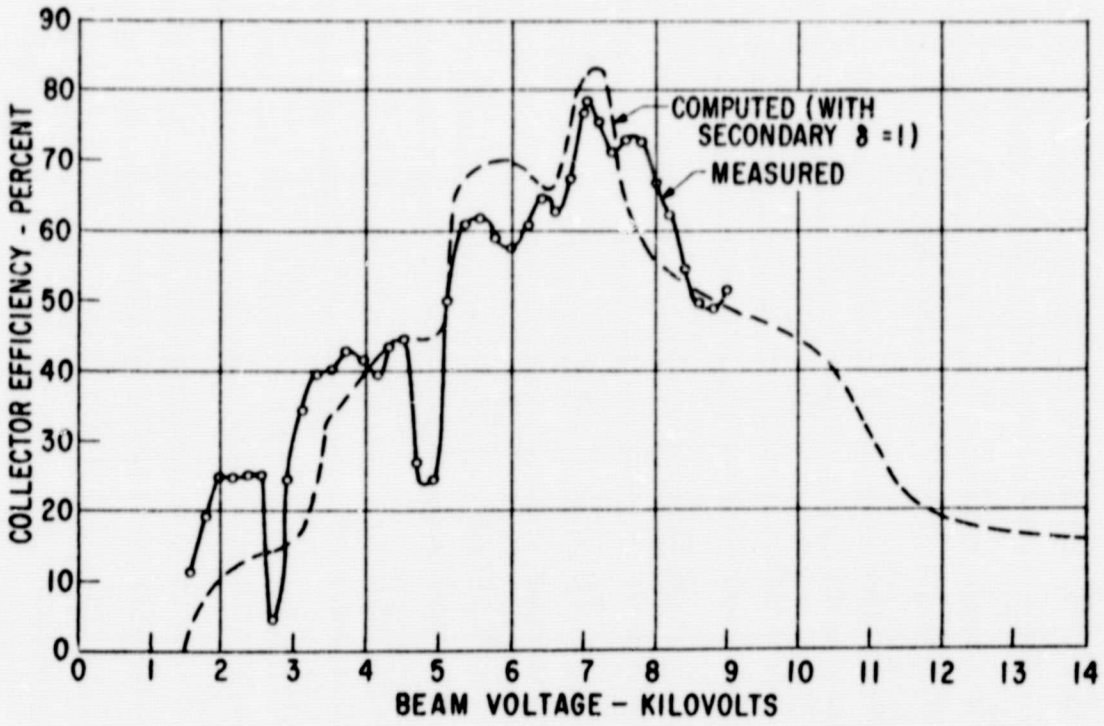

Comparison of Measured and Computed DC Efficiencies of Interim Collector

Under typical rf conditions the energies of electrons in the spent beam will extend from nearly zero energy to approximately twice the beam voltage, that is, up to 14 kv. We can estimate the rf performance of the collector by integrating to find the area under this curve and comparing it with the total area available. As you can see roughly one-third of the area of this figure is contained below the curves, so the high level rf collector efficiency should be about 35%. For less than full power output the output voltage swing will be reduced, and we can integrate about the 7 kv point to find the area under successively smaller portions of this curve. Doing this gives us curves of rf collector efficiency as a function of internal power output, as shown in the next slide.

In this slide rf collector efficiency is plotted as a function of rf power delivered to the output cavity. These measurements of collector efficiency versus power output were made by varying drive power, corresponding exactly to what would occur in an AM application. As you can see, the agreement between theory and measurement is quite good.

It was on the basis of the close correlation achieved on three levels between theory and experiment, as shown on the last four slides, that we felt we now had the tools and the understanding to attack the final collector design problem with confidence.

The next slide shows a sketch of the ten stage collector that was developed for the final design. Several new features deserve mention. Most important is the use of a suppressor grid just below the back cup to prevent secondaries from leaving the cup and arriving at lower potential electrodes.

Another difference between the interim collector and the final collector is the use of flat disk-shaped electrodes rather than conically-shaped

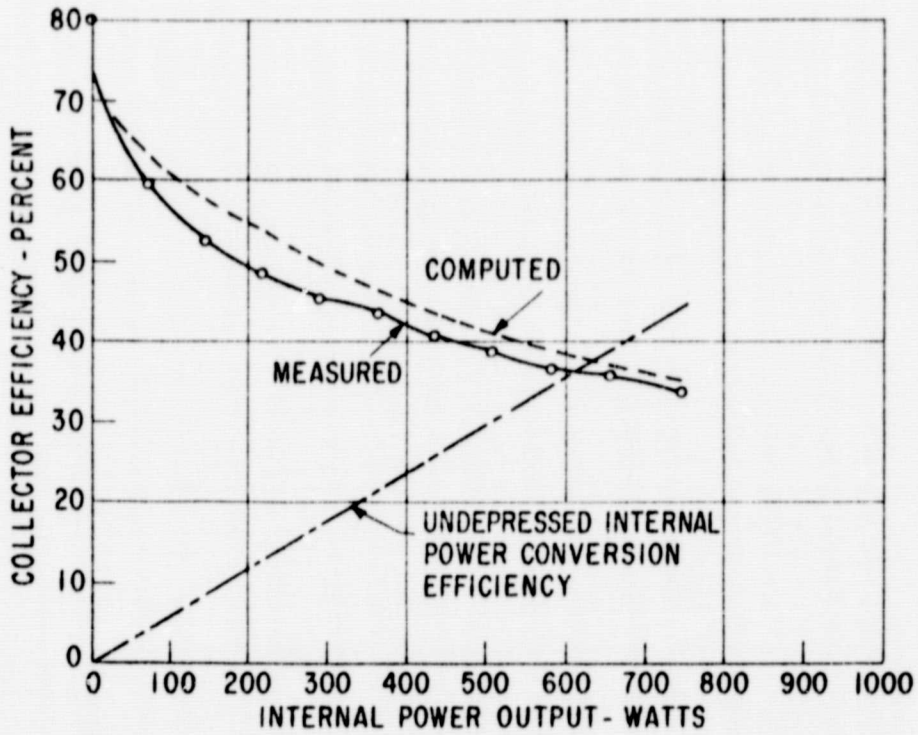

Measured and Computed RF Efficiency
of Interim Collector

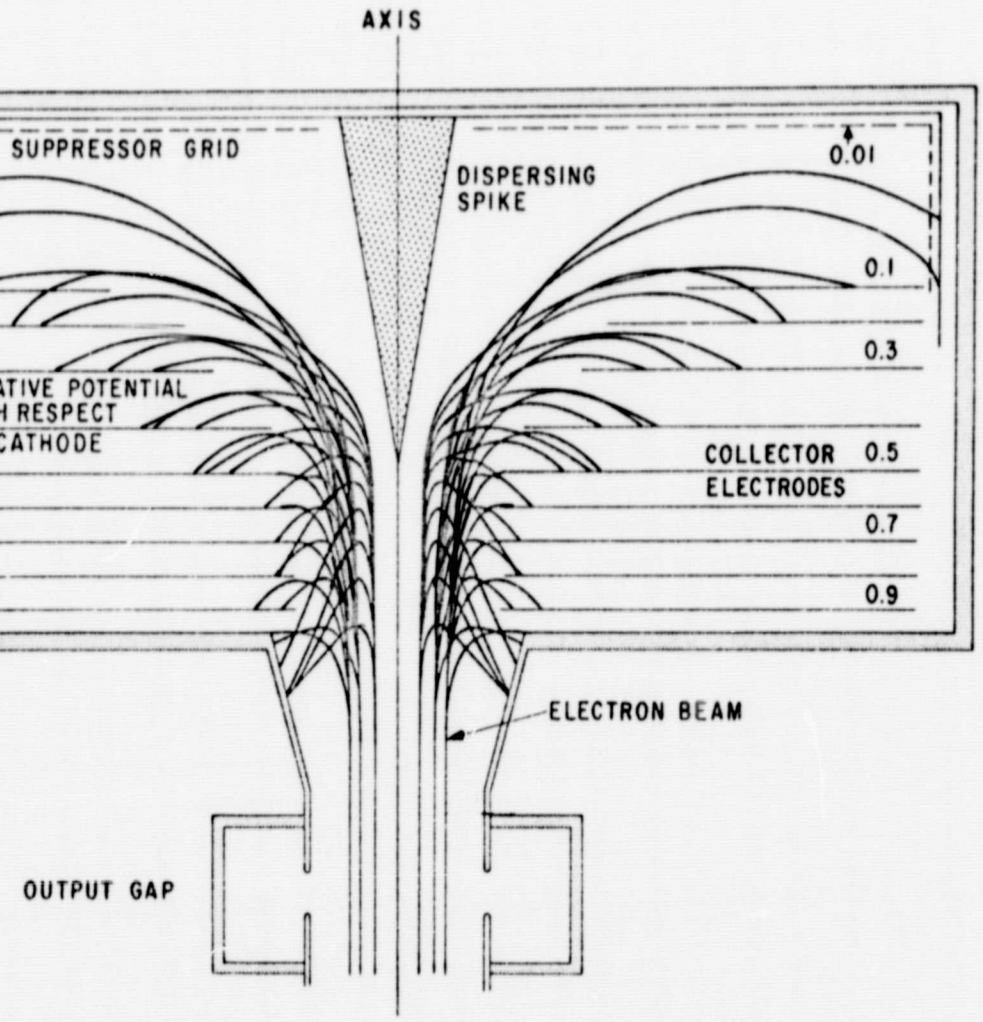

Electron Trajectories in the Final Collector, Starting with Parallel Flow

electrodes. Not only are these disks easier to fabricate, but they reduce bottomside hits which lead to energy absorption by secondary electrons.

The third difference between the collectors is that here the electrodes have been extended inward to reach somewhat closer to the beam than before. This was done on the basis of a detailed analysis of electron trajectories. This analysis also showed that a significant increase in efficiency could be made by increasing the number of electrodes from five to ten. These changes were all incorporated in the final design.

The single biggest unknown in collector design is the condition of the spent beam as it enters the collector region. This slide shows the trajectories calculated for a parallel beam entering the collector. We also ran a set of trajectories, shown in the next slide, which assumes a point source model for the spent beam. The optimum choice for the electrode edge locus depends critically upon which input conditions prevail in practice. Since this was unknown, an electrode edge locus finally was chosen which represented a compromise between the two choices.

We were now in a position to do a bean count to obtain a predicted curve for the dc collector efficiency of the final collector. The next slide shows the result. The solid line, obtained for the final collector, is a distinct improvement over the dashed line for the interim collector, taken from a previous slide. The improvement in the region from 7 kv to 14 kv is due primarily to the suppressor grid. The improvement in the region from 0 to 7 kv is due to a combination of the increase in electrode number from five to ten and of a more favorable electrode edge placement. Judging from the relative areas under these curves, we should expect a substantial improvement in rf collector efficiency as a result of the changes incorporated in the final collector.

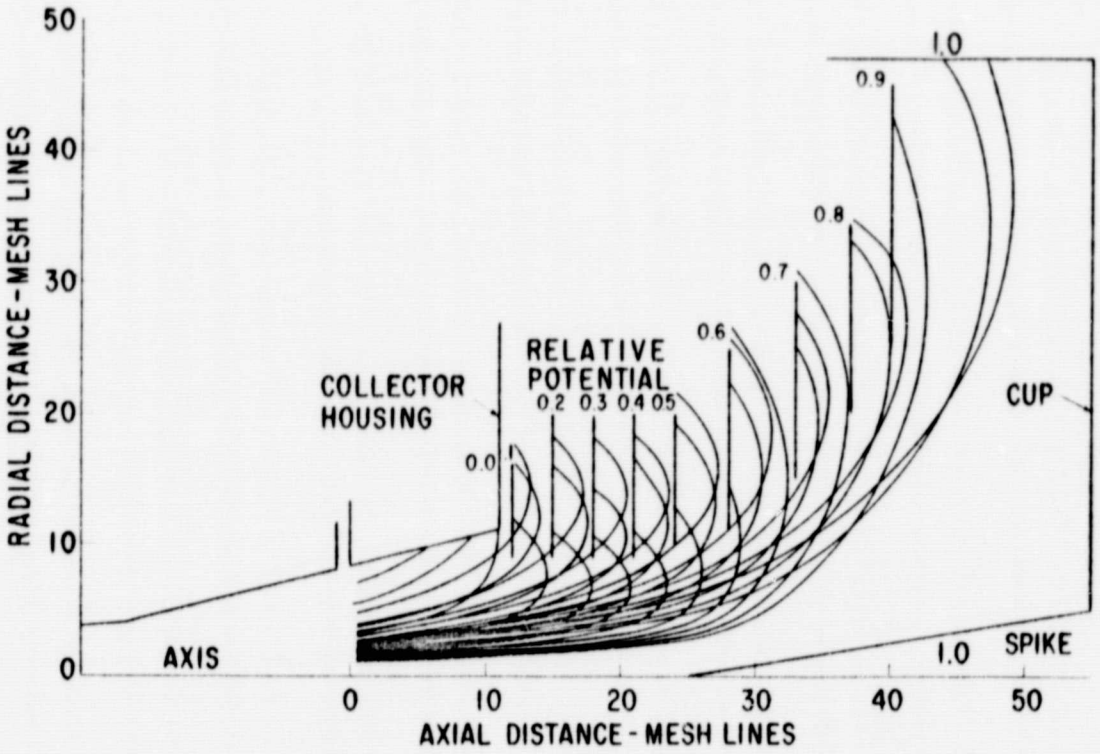

Final Collector Trajectories Starting from a Point Source

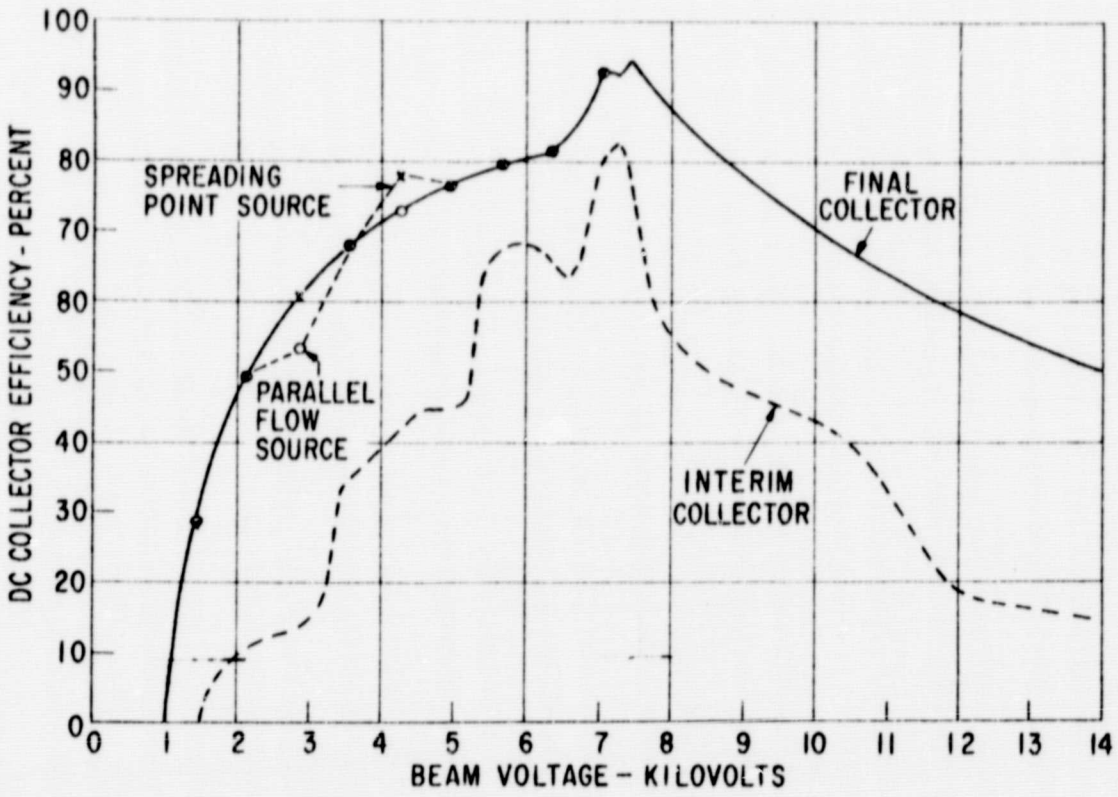

Comparison of Interim and Final Collector DC Efficiency

Before looking at the final rf performance curves, here is a slide which shows the construction of the final collector. The electrodes are suspended from individual feed-through insulators -- two per electrode. The only watercooled electrode is the back cup. Provision was made for water-cooling the spike, but this was found not to be necessary. The next slide is a photograph of the final collector attached to the tube and ready for testing.

The performance curve which best characterizes the final collector is, I think, this plot (next slide) of rf collector efficiency as a function of base tube efficiency. The final collector is computed to have a collector efficiency virtually double that of the interim collector, as shown by the upper dashed line.

Measurements of final collector efficiency, shown by the "x's" indeed all cluster just below the computed curve. If rf beam current interception is taken into account, as shown by the circles, the agreement becomes even better. For these data, base tube efficiency was varied by varying the drive power to the tube, exactly as would occur in AM service.

Perhaps the most significant advantage to be gained from the use of this collector in a practical application is that collector efficiencies of this magnitude allow a one-half to two-thirds reduction in the size of the heat rejection system.

The final slide shows the improvement in net tube efficiency as a function of base tube efficiency. Fifteen to 25 percentage points have been added to the base tube efficiency over the range shown here. To obtain this performance we had to use an auxiliary focusing coil between the output cavity and the collector. Without this coil the net tube efficiency at the highest output power would have been 65.3%.

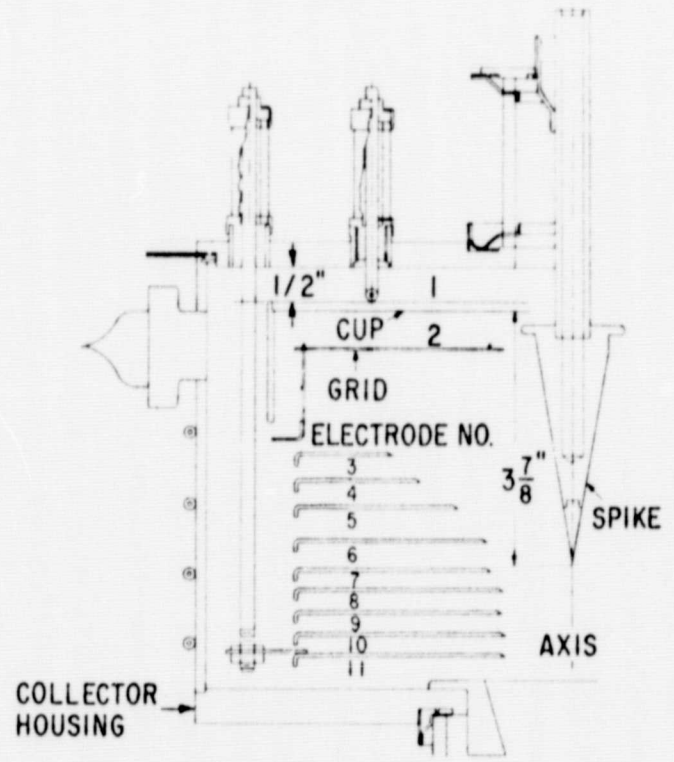

Final Collector Layout

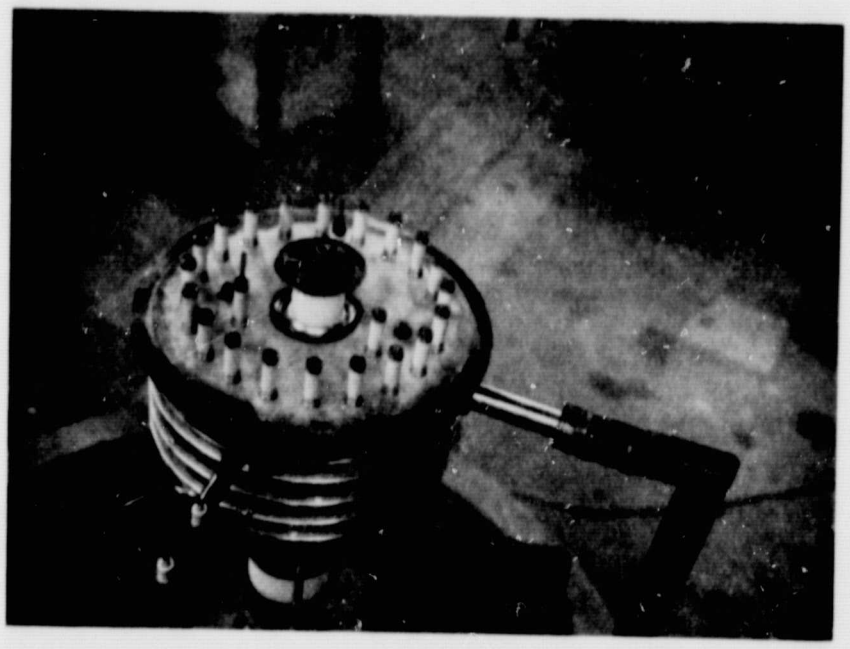

Assembled Collector and Tube on Exhaust Set

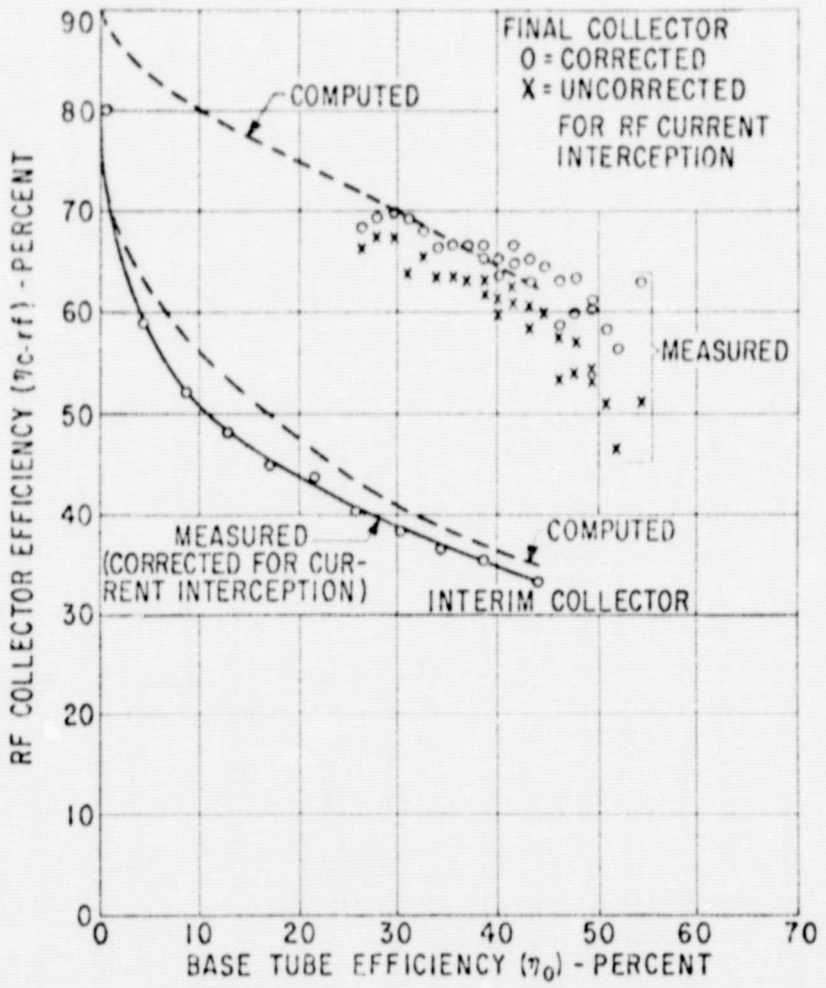

Comparison of Measured and Calculated RF Collector Efficiencies

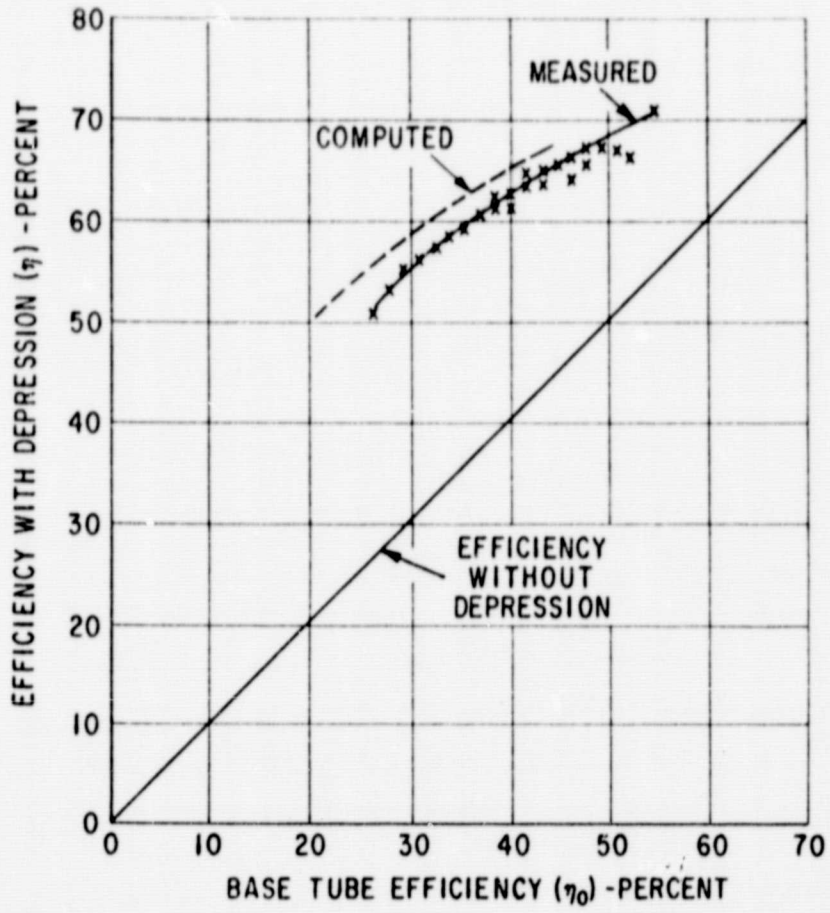

Net Tube Efficiency as a Function of Base Tube Efficiency

At this point it should be mentioned that the collector operation was very stable. There were no spurious oscillations and electron backstreaming was estimated to be less than 1%. The collector performance was also quite insensitive to changes in the electrode voltages. Changes as large as 5% in individual electrode voltages or even the intentional short circuiting of adjacent electrodes reduced the collector efficiency by less than 7%.

In summary, we have established a computational method for the design of depressed collectors which has predicted the measured performance of two electrostatic collectors. In the final collector over 60% of the energy of the spent beam of a klystron was recovered, and the net tube efficiency was raised by approximately twenty percentage points. More recent calculations have shown these figures do not represent the ultimate limit of depressed collector performance.

We would like to thank the NASA Lewis Research Center for their support of this work under Contract No. NAS3-11532.